# Evaluation of a Linear Phase Observation Operator with CHAMP Radio Occultation Data and High-Resolution Regional Analysis

S. SOKOLOVSKIY

*University Corporation for Atmospheric Research, Boulder, Colorado, and A.M. Obukhov Institute of Atmospheric Physics, Moscow, Russia*

Y.-H. KUO

*University Corporation for Atmospheric Research, and National Center for Atmospheric Research, Boulder, Colorado*

W. WANG

*National Center for Atmospheric Research, Boulder, Colorado*

(Manuscript received 19 May 2004, in final form 7 January 2005)

ABSTRACT

In this study a nonlocal, linear observation operator for assimilating radio occultation data is evaluated. The operator consists of modeling the excess phase, that is, integrating the refractivity along straight lines tangent to rays, below a certain height. The corresponding observable is the excess phase integrated through the Abel-retrieved refractivity, along the same lines, below the same height. The operator allows very simple implementation (computationally efficient) while accurately accounting for the horizontal refractivity gradients. This is due to significant cancellation of the linearization and discretization errors when modeling the observable. Evaluation of the operator with Challenging Minisatellite Payload (CHAMP) radio occultation data and grid refractivity fields from high-resolution regional analysis over the continental United States showed reduction of the observation error in the troposphere (below 7 km) 1.5–2 times, compared to the error of local refractivity. The operator is useful for the assimilation of radio occultation data by high-resolution weather models in the troposphere.

## 1. Introduction

Radio occultation (RO) remote sensing of the atmosphere, using Global Positioning System (GPS) and low earth orbiting (LEO) satellites, has the potential to become a valuable source of data for numerical weather prediction (NWP) and climate analysis in the future (Eyre 1994; Kursinski et al. 1997; Rocken et al. 1997; Anthes et al. 2000; Kuo et al. 2000). For example, the Constellation Observing System for Meteorology, Ionosphere and Climate (COSMIC) of six satellites, scheduled for launch in late 2005, will provide about 2500 globally distributed soundings per day (Rocken et al. 2000). Each RO sounding consists of profiles of the bending angle for the rays, traversing the neutral atmosphere, and the Abel-retrieved (AR) refractivity. The AR refractivity can be approximately assimilated as the local refractivity (which is related to pressure, temperature and humidity of air; Thayer 1974) at the estimated tangent points (TP) of the rays. However, this approximation may result in significant errors in the presence of strong horizontal refractivity gradients (fronts, strong convection, etc.), especially for high-resolution NWP models. The errors introduced by the horizontal gradients were studied by Gurvich and Sokolovskiy (1985), Gorbunov et al. (1996), Kursinski et al. (1997), Ahmad (1998), and Healy (2001). Accurate modeling of RO observables by ray tracing is computationally expensive (Liu and Zou 2003; Gorbunov and Kornblueh 2003; Poli and Joiner 2004). Alternative ap-

*Corresponding author address:* Sergey Sokolovskiy, 3300 Mitchell Lane, #3340, Boulder, CO 80301.
E-mail: sergey@ucar.edu

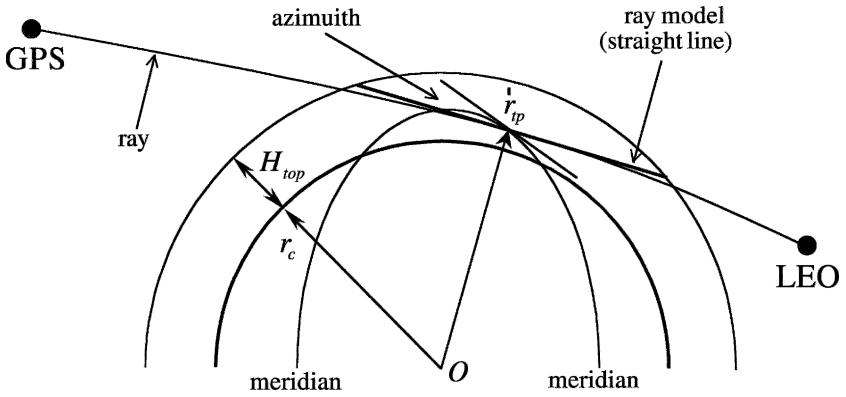


FIG. 1. Layout of the ray model (straight line) for the excess phase linear observation operator.

proaches consist of using simplified nonlocal observation operators that provide sufficient accuracy and are computationally efficient (Poli 2004; Sokolovskiy et al. 2005; Syndergaard et al. 2003, 2005).

In an earlier paper (Sokolovskiy et al. 2005) we introduced the nonlocal, linear, excess phase observation operator (i.e., refractivity integrated along straight lines, instead of rays, below the top of NWP model) and evaluated this operator by numerical simulations with a high-resolution (4 km) Weather Research and Forecasting (WRF) model. A significant reduction of the modeling errors, compared to modeling of the AR refractivity as the local refractivity, was demonstrated. In this study we evaluate the excess phase observation operator with real RO observations from the Challenging Minisatellite Payload (CHAMP) satellite (Wickert et al. 2001), the 10-km WRF model (Michalakes et al. 2001) forecasts, and 40-km National Centers for Environmental Prediction (NCEP) operational Eta analysis (Rogers et al. 1996) interpolated to the 10-km WRF grid.

Section 2 gives an overview of the excess phase observation operator (this operator is described in more detail by Sokolovskiy et al. (2005). Sections 3 and 4 give an overview of CHAMP RO data and WRF model grid fields used for evaluation of the observation operator. Section 5 presents the results of the evaluation. Finally, section 6 concludes the study.

## 2. The excess phase, linear observation operator

The idea behind simplified nonlocal observation operators is the use of relatively simple models of ray trajectories, which do not depend on the refractivity (Ahmad 1998). Such operators are linear functions of the refractivity and the ray tracing is unnecessary. The linearization, by itself, may introduce significant error. However, when modeling of an observable includes two steps and the same linearization is applied at both steps, this results in considerable reduction of the linearization errors due to their partial cancellation.

Modeling of the new observable, the excess phase path $S_{\mathrm{mod}}$, consists of integration of the 3D NWP refractivity $N_{\mathrm{mod}}(\mathbf{r})$ along straight lines tangent to rays at the estimated tangent points $\mathbf{r}_{\mathrm{tp}}$ below top height $\mathrm{H}_{\mathrm{top}}$, as shown in Fig. 1:

$$S_{\mathrm{mod}}(\mathbf{r}_{\mathrm{tp}}) = 10^{-6} \int N_{\mathrm{mo\,d}}(\mathbf{r})\, dl. \tag{1}$$

Syndergaard et al. (2003) suggested to invert $S_{\mathrm{mod}}(\mathbf{r}_{\mathrm{tp}})$ on the assumption of spherical symmetry of refractivity, thus modeling the AR refractivity $N_{ar}(r)$ more accurately than it can be modeled by local refractivity. In our approach we do not invert the phase, $S_{\mathrm{mod}}(\mathbf{r}_{\mathrm{tp}})$, instead, we calculate its observation counterpart $S_{\mathrm{obs}}(r_{\mathrm{tp}})$ by integrating the AR refractivity along the same straight lines below $H_{\mathrm{top}}$:

$$S_{\mathrm{obs}}(r_{\mathrm{tp}}) = 10^{-6} \int N_{\mathrm{ar}}(r)\, dl. \tag{2}$$

The new modeled variable (1) and its observation counterpart (2) approximately represent the true excess phase along the ray with a given TP and azimuth. Generally, the error of this approximation may be significant (due to ray bending), especially, in the troposphere. However, when the same approximation (straightline ray trajectories) is used in both (1) and (2), this results in substantial cancellation of the modeling errors when comparing (1) to (2). This was demonstrated by numerical simulations with high-resolution (4 km) WRF model by Sokolovskiy et al. (2005).

It is important to apply exactly the same finite-difference representation for numerical calculation of integrals (1) and (2). This results in substantial cancel-

TABLE 1. CHAMP occultations used for the evaluation study.

| Occultation day | Occultation time (UTC) | Lat (°) | Lon (°) | Azimuth (°) | Eta analysis time (UTC) |
|---|---|---|---|---|---|
| 6 Mar | 0538 | 37.0 | −93.6 | 169.7 | 0600 |
| 10 Mar | 0523 | 36.6 | −94.8 | 168.7 | 0600 |
| 12 Mar | 0515 | 36.4 | −95.5 | 168.3 | 0600 |
| 23 Mar | 0212 | 38.8 | −87.3 | −154.9 | 0300 |
| 31 Mar | 0139 | 39.7 | −89.3 | −156.6 | 0000 |
| 2 Apr | 0130 | 39.9 | −89.8 | −157.1 | 0000 |
| 4 Apr | 0122 | 39.4 | −89.9 | −157.1 | 0000 |
| 14 Apr | 0038 | 38.6 | −91.6 | −158.4 | 0000 |
| 22 Apr | 0001 | 37.6 | −92.7 | −159.1 | 0000 |
| 27 Apr | 2332 | 36.0 | −93.4 | −159.4 | 0000 (next day) |
| 29 Apr | 2323 | 35.6 | −93.6 | −159.5 | 0000 (next day) |

lation of the errors related to discretization of the observation operator. Another important point is related to the fact that in general (and, especially, with the application of radioholographic inversion methods; Gorbunov 2002; Jensen et al. 2003), RO provides higher vertical resolution than most NWP models. Thus, it is necessary to smooth $N_{\rm ar}(r)$ with a variable window, in order to make its resolution consistent with the vertical resolution of NWP model $N$. Such smoothing (filtering) allows for the reduction of the errors associated with aliasing of the small-scale structures of $N_{\rm ar}(r)$ into larger-scale vertical structures of $N_{\rm mod}(r)$, when assimilating RO data (Kuo et al. 2000, 2004).

The top height $H_{\rm top}$ can be chosen arbitrarily relatively to the height of ray tangent point $z_{\rm tp} = r_{\rm tp} - r_c$, which is subject to the following considerations. The length of the straight line below $H_{\rm top}$ must be sufficient for representing the effect of 3D $N$ irregularities in the excess phase. Thus, $H_{\rm top} - z_{\rm tp} \geq H_{\rm at}$, where $H_{\rm at}$ is the height of homogeneous atmosphere. Choosing $H_{\rm top} - z_{\rm tp}$ too small would introduce the error similar to the error of interpretation of the $N_{\rm ar}$ as the local $N$. On the other side, while the operators (1, 2) suppress high-frequency vertical harmonics of $N$ (this is good for high-frequency noise filtering), they exaggerate low-frequency harmonics (biases) proportionally to $H_{\rm top} - z_{\rm tp}$. Thus, $H_{\rm top} - z_{\rm tp}$ must not be significantly larger than $H_{\rm at}$. We note, that suppression of high-frequency vertical harmonics, when calculating $S$ from $N$, does not mean degrading RO observations since the original RO observable is the phase.

## 3. CHAMP radio occultation data

For this evaluation study we use the $N_{\rm ar}(z)$ obtained from CHAMP RO data (Wickert et al. 2001) processed by the COSMIC Data Analysis and Archive Center (CDAAC; Rocken et al. 2000). The CDAAC retrieval algorithms, described by Kuo et al. (2004), use the full spectrum inversion (Jensen et al. 2003) in the troposphere and the Doppler inversion above. For this study we use the occultations over the continental United States. We select the occultations with low rms observation noise ($<5 \times 10^{-6}$ rad in bending angle), descending to $z <$ km. For a single-case demonstration of the performance of the phase operator we use one occultation from June 2003. For statistical assessment of accuracy of the phase operator we use the occultations from March to April 2003. The spring period was chosen due to significant convective weather activity and strong horizontal $N$ gradients in the troposphere. The selection resulted in 11 occultations listed in Table 1. From each occultation we use $N_{\rm ar}$, latitude–longitude of TP and ray azimuth as functions of height $z$ over geoid, and the local curvature radius of the reference ellipsoid, $r_c$ under estimated occultation point.

To minimize the errors related to aliasing (see section 2), we first linearly interpolate $1{\rm n}N_{\rm ar}(r)$ to a dense vertical grid with constant spacing, then smooth by averaging with the window varying with height (consistent with the varying vertical resolution of the WRF grid) and interpolate $N_{\rm ar}(r)$ to a WRF-averaged vertical grid (see section 4).

## 4. High-resolution regional analysis

The National Center for Atmospheric Research (NCAR) Mesoscale and Microscale Meteorology (MMM) Division has been running the WRF model (Michalakes et al. 2001) for real-time prediction over the continental United States for the past 4 yr. The initial condition for the WRF model is obtained by interpolating the NCEP operational Eta analysis (Rogers et al. 1996; 40-km horizontal resolution, 26 pressure levels with 25- or 50-mb intervals) to the WRF grid (10-km horizontal resolution, 34 sigma levels in vertical, vertical resolution varying from ~0.1 km at surface to ~1 km at 20-km height). In this study, we use both the

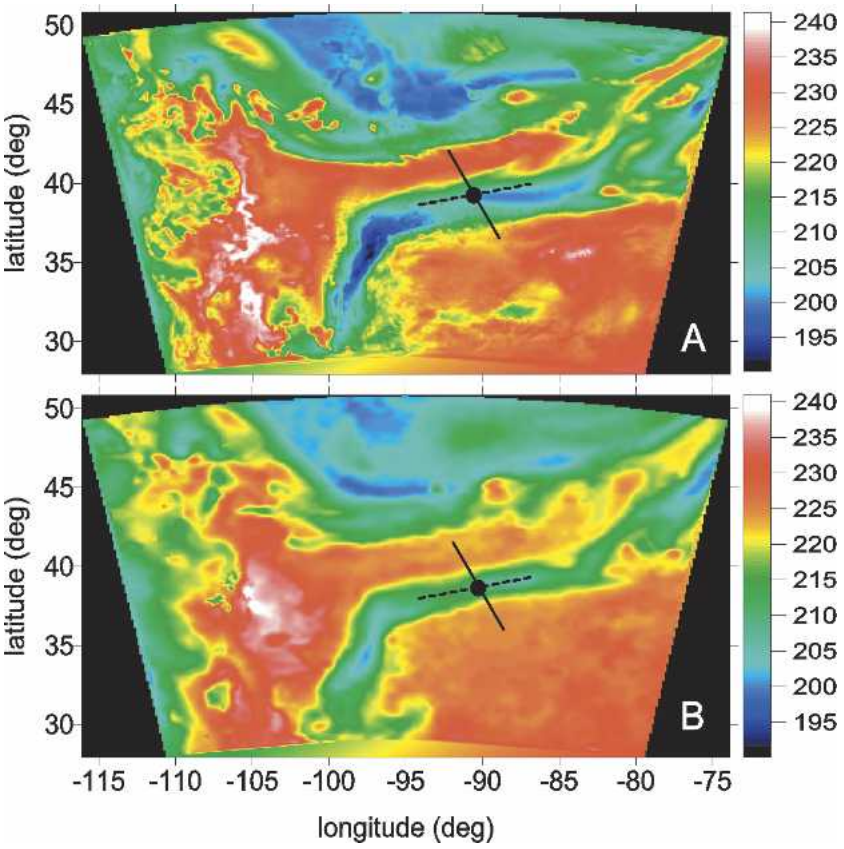


FIG. 2. Grid refractivity fields at 3.2-km height on 18 Jun 2003. (a) WRF 9-h forecast valid at 2100 UTC and (b) WRF/Eta analysis at 2100 UTC. Circle and solid line show location and azimuth of CHAMP occultation at 2036 UTC. Dashed line shows artificial azimuth used for calculation of the excess phase for comparison.

WRF forecast and the initial conditions for the WRF model interpolated from the 40-km Eta analysis (here, we call it WRF/Eta analysis for convenience) for 1 occultation in June 2003 and the WRF/Eta analysis at 3-h intervals for 11 occultations during the period of March–April 2003.

We calculate $N$ at the WRF model grid points, convert geopotential to geometric heights, and interpolate $N$ to one vertical grid, obtained by averaging all vertical grids over the selected domain, by cubic splines. We note that the interpolation of $N$ to a standard grid, generally, is not necessary and is used solely for simplifying calculations and comparisons of grid $N$ profiles in this evaluation study.

For integration of $N$ along straight lines we merge the 3D (latitude–longitude, height) grid $N$ field on top of the sphere with the radius $r_c$ (taken from RO inversion) and use constant integration step (5 km) along the lines. In this study we set $H_{\text{top}} = 15$ km because the difference in the vertical resolution of WRF model and Eta analysis above 15 km results in certain interpolation errors (this restriction is not essential and is related to only this study). For calculation of $N$ at an arbitrary point we apply linear interpolation in vertical and simple horizontal interpolation $N = \Sigma\, c_i N_i$, $i = 1, 2, 3, 4$, where $N_i$ are the refractivities at four corner pixels and the coefficients $c_i$ are inverse proportional to distances to those pixels ($\Sigma\, c_i = 1$). Such interpolation is rather coarse, but small horizontal spacing and, most important, application of the same interpolation for (1) and (2) makes the result fairly insensitive to interpolation scheme.

## 5. Results

At first, we illustrate the performance of the nonlocal excess phase observation operator by use of one occultation that occurred over the region with strong horizontal along-track $N$ gradient in the troposphere at 2036 UTC 18 June. For this occultation we use both the WRF forecast and the WRF/Eta analysis. Figure 2 shows the 2D refractivity field at 3.2-km height: 10-km

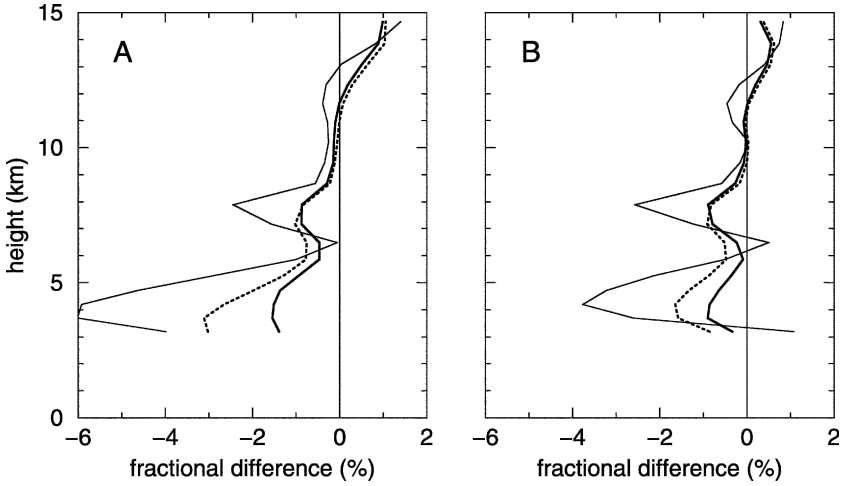


FIG. 3. Refractivity (thin lines) and excess phase (bold lines) observation errors for CHAMP occultation at 2036 UTC 18 Jun compared to (a) WRF 9-h forecast started at 1200 UTC, valid at 2100 UTC and (b) WRF/Eta analysis at 2100 UTC. Dashed lines show the excess phase observation error for the artificially directed straight lines (see text and Fig. 2).

WRF 9-h forecast started at 1200 UTC (Fig. 2a) and WRF/Eta analysis (Fig. 2b), both valid at 2100 UTC 18 June. Location and azimuth of the occultation are shown by circle and solid line. The location corresponds to bottom height, but for modeling of the excess phase we use the individual location of TP at each height. Figure 3 shows the refractivity and the excess phase observation errors, $\Delta N(\mathbf{r}_{tp}) = [N_{ar}(r_{tp}) - N(\mathbf{r}_{tp})]/N(\mathbf{r}_{tp})$ (thin line) and $\Delta S(\mathbf{r}_{tp}) = [S_{obs}(r_{tp}) - S_{mod}(\mathbf{r}_{tp})]/S(\mathbf{r}_{tp})$ (bold line) for the WRF forecast (Fig. 3a) and the WRF/Eta analysis (Fig. 3b). Since the occultation is located in the "valley" of the refractivity, the local refractivity has significant negative error. This error is substantially reduced in the excess phase, in particular, due to accounting for horizontal along-track $N$ gradients. The fractional reduction of the error is about the same for the forecast and the analysis. Dashed lines show the errors of the excess phase when it was calculated along straight lines not tangent to the rays, but artificially directed along the valley, as shown by dashed lines in Fig. 2. This results in increase of the error by a factor of 1.5–2 below 6 km, thus illustrating the importance of accounting for the horizontal $N$ gradients in the nonlocal observation operator.

Table 1 shows times, TP locations (latitude–longitude) and ray azimuths for the 11 occultations from March to April 2003, and the corresponding times of the WRF/Eta analysis used for the evaluation. Figure 4 shows the results of statistical evaluation of the errors for the 11 selected occultations. Figure 4a shows the fractional standard deviation of the refractivity $\Sigma_N = \langle (N - \langle N \rangle)^2 >^{1/2} / \langle N \rangle$, where $\langle\ \rangle$ denotes averaging over the ensemble (curve 1), the fractional mean error $\mu_N = \langle \Delta N \rangle / \langle N \rangle$ (curve 2), and the fractional standard error $\sigma_N = \langle (\Delta N - \langle \Delta N \rangle)^2 >^{1/2} / \langle \Delta N \rangle$ (curve 3). Similarly, Fig. 4b shows the fractional standard deviation $\Sigma_S$ (curve 1), the fractional mean $\mu_s$ (curve 2), and the fractional standard error $\sigma_S$ (curve 3) of the excess phase. Figure 4c shows the number of occultations penetrating down to a given height. We note that the 95% confidence intervals for 6 events (between 2 and 4 km) and for 11 events (above 4 km) is $1.94\sigma$ and $1.8\sigma$ correspondingly, not significantly different from the confidence interval for an infinite number of events, $1.65\sigma$ (Martin 1971). Thus, we consider the results statistically significant at 95% confidence level. As seen from Figs. 4a,b, generally, $\sigma_S < \sigma_N$. This fact by itself, without separate estimation of the measurement, modeling, and representativeness errors that compose the observation error (we adhere to the error definition introduced in earlier paper by Sokolovskiy et al. 2005), does not provide sufficient evidence of the advantage of the $S$ operator over the local $N$. In this study such evidence is provided by reduction of the observation error not only in fraction of the mean observable, but, also, in fraction of its standard deviation. The standard deviation of an observable can be considered as an estimate of the magnitude of the weather-induced atmospheric variability projected into the observation space. The fact that not only $\sigma_S/\sigma_N < 1$ but, also, $(\sigma_S/\Sigma_S)/(\sigma_N/\Sigma_N) < 1$, means that the atmospheric variability can be represented better, that is, with smaller observation error, by use of $S$ than of the local $N$, regardless of partitioning of the observation error into the measurement, modeling, and rep-

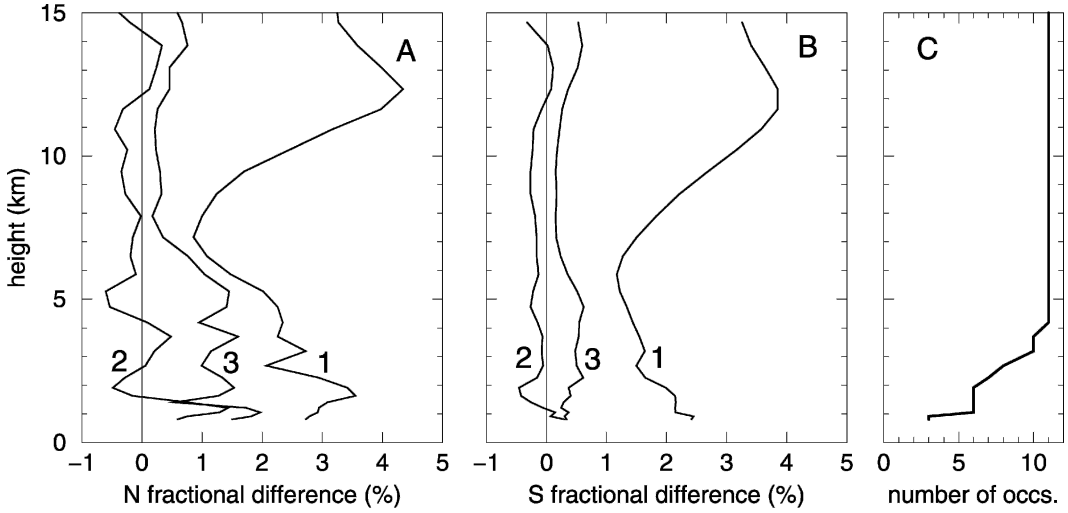


FIG. 4. Standard deviations (curves 1) and mean and standard errors (curves 2 and 3) of (a) the refractivity and (b) the excess phase for 11 CHAMP occultations (for details see text). (c) The number of occultations penetrating to a certain height.

resentativeness errors (i.e., independent estimation of their magnitudes). This indicates that the use of the nonlocal linear excess phase observation operator is advantageous in the troposphere (cf. local refractivity).

As seen from Figs. 4a,b, there is a region of large fractional variability of $N$ and $S$ (larger than in the troposphere), at ~12-km height. Apparently, this is caused by variations of the height of tropopause. But since the moisture is low at that height, the horizontal $N$ gradients, caused mainly by density gradients, are low. As a result, the errors of local refractivity are small and the use of nonlocal observation operators in this region is not so advantageous as in the troposphere.

## 6. Conclusions

The excess phase observation operator for assimilating RO data is a simple nonlocal, linear (with respect to refractivity) operator, which accounts for horizontal refractivity gradients. Despite its simplicity, this operator results in significant reduction of the observation errors in the troposphere, compared to local refractivity. It is important to use the same discretization, when modeling the excess phase from 1D RO AR refractivity and from 3D NWP refractivity. This allows for substantial cancellation of the modeling errors, by not requiring application of highly accurate and complicated interpolation schemes, and thus making the observation operator fairly simple for practical implementation and computationally efficient. It is also important to make the vertical resolution of RO observations and NWP model consistent (generally, by smoothing RO refractivity). This allows for minimization of the errors related to aliasing.

Evaluation of the linear excess phase observation operator with CHAMP RO data and high-resolution WRF model forecast and WRF/Eta regional analysis over the continental United States for the June 2003 case demonstrated the importance of accounting for the horizontal refractivity gradients along the ray, which are not accounted for by the local refractivity observation operator. Statistical evaluation by use of 11 GPS RO soundings selected during the period of March–April 2003 demonstrated reduction of the observation error of the excess phase compared to the error of local refractivity in the troposphere, below 7 km. The reduction of the observation error in fraction of the mean observable is ~2 times, and in fraction of the standard deviation of the observable it is ~1.5 times.

These results indicate that the use of the nonlocal excess phase observation operator is advantageous for high-resolution (horizontal resolution <100 km) mesoscale NWP models in the troposphere, where there are significant refractivity gradients. Above the troposphere, due to low moisture and smaller horizontal refractivity gradients, the use of the excess phase does not result in significant error reduction compared to local refractivity.

*Acknowledgments.* This work was supported by the National Science Foundation (NSF) as part of development of the Constellation Observing System for Meteorology Ionosphere and Climate (COSMIC) Data Analysis and Archive Center (CDAAC) at UCAR, the

NSF Office of Polar Programs (OPP) Grant NSF OPP-0230361, under Cooperative Agreement ATM-9732665, the Office of Naval Research, Code 322MM, and NASA through Grant NAG 5-9518 to Ohio State University and UCAR.

## REFERENCES

Ahmad, B., 1998: Accuracy and resolution of atmospheric profiles obtained from radio occultation measurements. Scientific Rep. DPD811-1988-1, Center for Radar Astronomy, Stanford, CA, 123 pp.

Anthes, R. A., C. Rocken, and Y.-H. Kuo, 2000: Application of COSMIC to meteorology and climate. *Terr. Atmos. Ocean Sci.,* **11,** 115–156.

Eyre, J. R., 1994: Assimilation of radio occultation measurements into a numerical weather prediction system. European Centre for Medium-Range Weather Forecasts, Tech. Memo. 199, 34 pp.

Gorbunov, M. E., 2002: Canonical transform method for processing radio occultation data in the lower troposphere. *Radio Sci.,* **37,** 1076, doi:10.1029/2000RS002592.

——, and L. Kornblueh, 2003: Principles of variational assimilation of GNSS radio occultation data. Max Planck Institute for Meteorology Rep. 350, 34 pp.

——, S. V. Sokolovskiy, and L. Bengtsson, 1996: Space refractive tomography of the atmosphere: Modeling of direct and inverse problems. Max Planck Institute for Meteorology Rep. 210, 59 pp.

Gurvich, A. S., and S. V. Sokolovskiy, 1985: Reconstruction of a pressure field by remote refractometry from space. *Izv. Atmos. Ocean Phys.,* **21,** 7–13.

Healy, S. B., 2001: Radio occultation bending angle and impact parameter errors caused by horizontal refractive index gradients in the troposphere: A simulation study. *J. Geophys. Res.,* **106** (D11), 11 875–11 889.

Jensen, A. S., M. S. Lohmann, H.-H. Benzon, and A. S. Nielsen, 2003: Full spectrum inversion of radio occultation signals. *Radio Sci.,* **38,** 1040, doi:10.1029/2002RS002763.

Kuo, Y.-H., S. V. Sokolovskiy, R. A. Anthes, and F. Vandenberghe, 2000: Assimilation of GPS radio occultation data for numerical weather prediction. *Terr. Atmos. Ocean Sci.,* **11,** 157–186.

——, T.-K. Wee, S. Sokolovskiy, C. Rocken, W. Schreiner, D. Hunt, and R. A. Anthes, 2004: Inversion and error estimation of GPS radio occultation data. *J. Meteor. Soc. Japan,* **82** (1B), 507–531.

Kursinski, E. R., G. A. Hajj, J. T. Schofield, R. P. Linfield, and K. R. Hardy, 1997: Observing Earth's atmosphere with radio occultation measurements using the Global Positioning System. *J. Geophys. Res.,* **102** (D19), 23 429–23 465.

Liu, H., and X. Zou, 2003: Improvements to a GPS radio occultation ray-tracing model and their impacts on assimilation of bending angle. *J. Geophys. Res.,* **108,** 4548, doi:10.1029/2002JD003160.

Martin, B. R., 1971: *Statistics for Physicists*. Academic Press, 209 pp.

Michalakes, J., S. Chen, J. Dudhia, J. Klemp, J. Middlecoff, and W. Skamarock, 2001: Development of a next generation regional weather research and forecast model: Developments in teracomputing. *Proceedings of the Ninth ECMWF Workshop on the Use of High Performance Computing in Meteorology,* W. Zwiefthofer and N. Kreitz, Eds., World Scientific, 269–276.

Poli, P., 2004: Effects of horizontal gradients on GPS radio occultation observation operators. II: A fast atmospheric refractivity gradient operator. *Quart. J. Roy. Meteor. Soc.,* **130,** doi:10.1256/qj.03.229.

——, and J. Joiner, 2004: Effects of horizontal gradients on GPS radio occultation observation operators. I: Ray tracing. *Quart. J. Roy. Meteor. Soc.,* **130,** doi:10.1256/qj.03.228.

Rocken, C., and Coauthors, 1997: Analysis and validation of GPS/MET data in the neutral atmosphere. *J. Geophys. Res.,* **102** (D25), 29 849–29 866.

——, Y.-H. Kuo, W. Schreiner, D. Hunt, S. Sokolovskiy, and C. McCormick, 2000: COSMIC system description. *Terr. Atmos. Ocean Sci.,* **11,** 157–186.

Rogers, E., T. Black, D. Deaven, G. DiMego, Q. Zhao, M. Baldwin, N. Junker, and Y. Lin, 1996: Changes to the operational "early" Eta analysis/forecast system at the National Centers for Environmental Prediction. *Wea. Forecasting,* **11,** 391–413.

Sokolovskiy, S., Y.-H. Kuo, and W. Wang, 2005: Assessing the accuracy of a linearized observation operator for assimilation of radio occultation data: Case simulations with a high-resolution weather model. *Mon. Wea. Rev.,* **133,** 2200–2212.

Syndergaard, S., D. Flittner, R. Kursinski, and B. Herman, 2003: Simulating the influence of horizontal gradients on refractivity profiles from radio occultations. *Proc. Fourth Oersted Int. Science Team Conf. (OIST-4),* Copenhagen, Denmark, Danish Meteorological Institute, 245–250.

——, E. R. Kursinski, B. M. Herman, E. M. Lane, and D. E.Flittner, 2005: A refractive index mapping operator for assimilation of occultation data. *Mon. Wea. Rev.,* **133,** 2650–2668.

Thayer, G. D., 1974: An improved equation for the radio refractive index of air. *Radio Sci.,* **9,** 803–807.

Wickert, J., and Coauthors, 2001: Atmosphere sounding by GPS radio occultation: First results from CHAMP. *Geophys. Res. Lett.,* **28,** 3263–3266.